

Article

Half-Metallicity and Magnetism of the Quaternary Heusler Compound $\text{TiZrCoIn}_{1-x}\text{Ge}_x$ from the First-Principles Calculations

Ying Chen ^{1,*}, Shaobo Chen ¹ , Bin Wang ², Bo Wu ³ , Haishen Huang ³, Xinmao Qin ¹, Dongxiang Li ¹ and Wanjun Yan ¹

¹ School of Mathematics and Physics, Anshun College, Anshun 561000, China; shaobo.chen@yeah.net (S.C.); qxm200711@162.com (X.Q.); ldx0601@163.com (D.L.); yanwanjun7817@163.com (W.Y.)

² Anshun first senior high school, Anshun 561000, China; wangcowley@163.com

³ Department of Physics, Zunyi Normal College, Zunyi 563002, China; fqwubo@163.com (B.W.); hhs_vir@yeah.net (H.H.)

* Correspondence: ychenjz@163.com

Received: 16 January 2019; Accepted: 8 February 2019; Published: 13 February 2019



Abstract: The effects of doping on the electronic and magnetic properties of the quaternary Heusler alloy TiZrCoIn were investigated by first-principles calculations. Results showed that the appearance of half-metallicity and negative formation energies are associated in all of the $\text{TiZrCoIn}_{1-x}\text{Ge}_x$ compounds, indicating that Ge doping at Z-site increases the stability without damaging the half-metallicity of the compounds. Formation energy gradually decreased with doping concentration, and the width of the spin-down gap increased with a change in Fermi level. $\text{TiZrCoIn}_{0.25}\text{Ge}_{0.75}$ was found to be the most stable half-metal. Its Fermi level was in the middle of the broadened gap, and a peak at the Fermi level was detected in the spin majority channel of the compound. The large gaps of the compounds were primarily dominated by the intense d-d hybridization between Ti, Zr, and Co. The substitution of In by Ge increased the number of sp valence electrons in the system and thereby enhanced RKKY exchange interaction and increased splitting. Moreover, the total spin magnetic moments of the doped compounds followed the Slater–Pauling rule of $M_t = Z_t - 18$ and increased from $2 \mu_B$ to $3 \mu_B$ linearly with concentration.

Keywords: quaternary Heusler alloy; doping; spin polarization; half-metallicity; magnetism

1. Introduction

Half-metallic ferromagnets [1–4] are potential candidates for spintronic applications owing to their completely spin-polarized band structures [5–8]. Of all known materials exhibiting half-metallicity, Heusler alloys have attracted considerable interest because of their high spin magnetic moments and high Curie temperatures [9–11]. Original and stoichiometric full-Heusler alloys have X_2YZ in their chemical formulas, where X and Y denote transition metal elements and Z is a primary group element. These Heuslers usually crystalize with a cubic $L2_1$ structure (space group $Fm-3m$, No. 255) and individually contain four interpenetrating fcc sublattices in their ideal forms. Several theoretical and experimental studies confirmed a series of Heusler compounds with half-metallicity [12–15]. Recently, quaternary Heusler alloys have increasingly attracted interest [16–21] owing to their half-metallicity and spin gapless band structures. These compounds show a distinct structural symmetry (space group $F-43m$, No. 216) resulting from the partial replacement of X in X_2YZ by another element X' . This crystal structure can be defined as a LiMgPdSn prototype. Most of these compounds, such as $\text{Co}_2\text{Mn}_{1-x}\text{Fe}_x\text{Si}$, were designed for adjusting the Fermi energy to the middle of the gap [22]. Equivalent stoichiometric quaternary Heusler alloys have been extensively researched. CoFeMnZ compounds

(Z=Al, Ga, Si, or Ge) with 1: 1: 1: 1 stoichiometries show half-metallicity [23]. Özdoğan et al. performed a theoretical study on 60 LiMgPdSn-type quaternary Heusler alloys and found that most of the alloys exhibit half-metallicity [24]. Ideal properties, such as stable half-metallicity, large spin magnetic moment, and high Curie temperature, can be observed in the ordered bulk phase. Unfortunately, temperature, impurity, and other external factors can disrupt the completely spin-polarized band structures and further degrade the half-metallicity of ideal compounds [25–34]. For example, in the traditional full Heusler compound Co_2MnSi , a remarkable gap with 0.4 eV in minority band at 985 K may disappear, and only a spin polarization of 61% can be observed at a barrier interface consisting of a single electrode made of a Co_2MnSi film [35–38].

A dramatically large spin-down gap of 0.93 eV was detected in a quaternary Heusler TiZrCoIn [39]. The Ti of this compound was inclined to sit at $A(0, 0, 0)$, Zr at $B(0.25, 0.25, 0.25)$, Co at $C(0.5, 0.5, 0.5)$, and In at $Z(0.75, 0.75, 0.75)$ in the Wyckoff position coordinate. This compound might be an excellent candidate for spin-injectors because of its extraordinary wide band gap. Its performance for spintronic applications can be enhanced by modulating its magnetic and electronic properties on the basis of valence-electron count. In the present work, we searched for a mixed compound in the series $\text{TiZrCoIn}_{1-x}\text{Ge}_x$ where the half-metallic behavior is stable against the variation of impurity.

2. Calculation Methods

First-principles calculations were performed with the CASTEP code on the basis of the density functional theory (DFT). The stable ground structure of quaternary Heusler alloy TiZrCoIn was obtained by optimizing the structure. On the basis of the stable ground structure, one, two, three, or four Ge atoms were used to replace In atoms in a unit cell. Doping concentrations of 25%, 50%, 75%, and 100% were obtained. For the simulation of small doping concentrations of 12.5%, 6.25%, and 3.125%, TiZrCoIn supercells with 32, 64, and 128 atoms, respectively, were produced. The In atom was replaced by one Ge atom. Then, the correlation property calculations, such as the single point energy, density of states (DOS), and band-structure, were performed on the minimized doped cases obtained from the geometry optimization. In our calculations, all the electronic structure calculations were performed with the spin polarization. Generalized gradient approximation parameterized by Perdew [40,41] were used for the handling of the exchange and correlation term. Electron–ion interactions were disposed with ultrasoft pseudopotentials [42]. In the SCF calculation, a refined 11×10^{-6} eV/atom was used as a convergence criterion. For the energy cutoff of the planewave, the basis was set to 310 eV. The calculation was considered converged when the largest gradient was less than $0.002 \text{ eV}/\text{\AA}$. In the property calculations, the $7 \times 7 \times 7$ special k-mesh points in Brillouin zone were applied. The electrons of Ti $3d^24s^2$, Zr $4d^25s^2$, Co $3d^74s^2$, In $5s^25p^1$, and Ge $4s^24p^2$ were regarded as valence electrons.

3. Results and Discussion

3.1. Formation Energy of Doped TiZrCoIn

The formation energy of the doped systems were analyzed with respect to the ordered case and estimated by using formula

$$E_f(dop) = E(dop) - E(\text{TiZrCoIn}) - \sum m_i \mu_i(\text{bulk}) \quad (1)$$

where $E(dop)$ is the total energy of the doped case, and $E(\text{TiZrCoIn})$ is the total energy of the ordered TiZrCoIn structure in the same supercell size. The last term $\sum m_i \mu_i(\text{bulk})$ can be derived from the number of atoms added or removed from the ideal alloy. The number of altered atoms relative to that in the ideal bulk is represented by m_i , which is either positive, when atoms are added to the original system, or negative, when atoms are removed from system. The symbol $\mu_i(\text{bulk})$ stands for the chemical potential of the corresponding atom in its bulk phase of ground state. Experimental

preparation conditions and annealing environment can affect the formation of these doped systems. Thus, the formation energy of a doped structure is influenced by the chemical potential of the host atoms, which are affected by the environment. To obtain the chemical potentials from their bulk phase, we assumed that Ti, Zr, Co, In, and Ge are in the thermodynamic equilibrium with their bulk solid phase in the host rich condition. The hcp, hcp, hcp, fcc, and fcc structures for the bulk phases of Ti, Zr, Co, In, and Ge, respectively, were adopted.

The formation energy of each doped system was calculated with the formula above. The results are shown in the first column of Table 1. All the doped systems had negative formation energies. Thus, In atoms in the ordered phase were easily replaced by Ge atoms. The ideal bulk of TiZrCoIn alloy was affected by the impurity Ge during growth. The variations among these values indicated differences in stability. Lower formation energy indicates that the doped one is easier to be formed spontaneously during the growth. It is shown in table 1 the formation energy gets smaller with the doping concentration, which manifests the doped system tends to be formed at a high doping concentration. The highest formation energy was obtained at a doping concentration of 3.125%. However, it can still form spontaneously during growth owing to its negative formation energy (−9.256 eV). The lowest formation energy was obtained at 100% doping concentration. Hence, the doped compound (TiZrCoGe) is most likely to be fabricated experimentally compared to the other Ge doped compounds. Meanwhile, Ge doping at Z-site may further stabilize the compound.

Table 1. Formation energies (E_f), lattice parameters (unit in Å), spin polarizations presented as spin-up over spin-down ratios, width of spin-down gap around the Fermi level (in units of eV), and total magnetic moments in a unit cell. Notice that x is the doping concentration.

x	E_f (eV)	a (Å)	$P(\frac{\uparrow-\downarrow}{\uparrow+\downarrow})(\%)$	Band Gap (eV)	M_t ($\mu_B/f.u.$)
x = 0	-	6.562	100	0.914	1.99
x = 3.125%	−9.256	6.633	100	0.681	2.03
x = 6.25%	−9.280	6.630	100	0.692	2.06
x = 12.5%	−9.333	6.609	100	0.721	2.13
x = 25%	−9.435	6.566	100	0.802	2.26
x = 50%	−9.604	6.496	100	0.904	2.50
x = 75%	−9.776	6.427	100	0.960	2.75
x = 100%	−10.109	6.356	100	1.130	3.00

3.2. Electronic Structure: Magnetic Moments and DOS

The quaternary Heusler compound TiZrCoIn with the configuration mentioned above showed half-metallic property and a broad indirect spin-down gap of 0.914 eV at the equilibrium lattice constant of 6.562 Å. This result fits perfectly with the previous prediction in Reference [39]. Lattice parameters, spin polarizations, width of spin-down gap, and total magnetic moments in a unit cell are listed in Table 1. The spin polarizations at the Fermi levels of all the doped structures were 100%. Thus, all the derived compounds were half-metal. In addition, the magnetic moments increased from 2 μ_B to 3 μ_B at increased doping concentration.

Before the detailed analysis of doping functional mechanism in quaternary Heusler TiZrCoIn, we initially discuss the ideal case of the compound TiZrCoIn. The spin-polarization total DOS and the atom PDOS are presented in the first line of Figures 1 and 2, respectively. In Figure 1, the spin-up band (shadowed area) of compound TiZrCoIn with ordered structure was metallic. Meanwhile, a wide energy gap was observed in the spin-down band at the Fermi level. The electrons at the Fermi level were totally polarized, and this condition resulted in 100% spin polarization. The width of the band gap was 0.914 eV, and the Fermi level was slightly near the bottom of the band gap. Thus, the half-metallicity of quaternary Heusler TiZrCoIn was susceptible to external influences. Meanwhile, the gap was primarily determined by the covalent hybridization between Ti and Co, as shown in Figure 2. The d states of Ti with low valence occupied the high energy area above the Fermi level, thereby forming the bonding bands. By contrast, the d states of Co with high valence were located at

the low energy area below the Fermi level, thereby forming the antibonding bands. Ti and Co atoms have the same symmetry as in typical $L2_1$ full-Heuslers, and thus their d orbitals hybridize initially and form five bonding d hybrids and five nonbonding ones. Then, the five bonding d hybridized orbitals of Ti-Co hybridize with the d orbitals of the Zr atoms, thereby regenerating bonding and antibonding states. Given the large energy separation of d hybrids of the Ti and Co atoms, the five nonbonding d hybrids Ti-Co, namely, the t_{1u} and e_u states, possess high energies and are unoccupied. A detailed d-d hybridization diagram is shown in Figure 3. Introduced by the sp element In, a single degenerate s band and a triple degenerated p band, lying deep in energy, are located below the d states and accommodate d charge from the transition metal atoms. Thus, 9 instead of 12 occupied states are usually observed in the spin-down band. In the quaternary Heusler alloy TiZrCoIn, the In atom carried three valence electrons, and Ti, Zr, and Co carried four, four, and nine, respectively. Therefore, 17 transition metal electrons were found, of which 5 were cached by the s and p bands of the In atom, 10 were filled in the bonding d bands, and 2 were uncompensated. Thus, a total spin magnetic moment of $2 \mu_B$ was observed in the compound TiZrCoIn. The total magnetic moments followed the Slater–Pauling rule: $M_t = Z_t - 18$, where M_t represents the total spin magnetic moments in a unit cell, and Z_t is the number of the total valence electron.

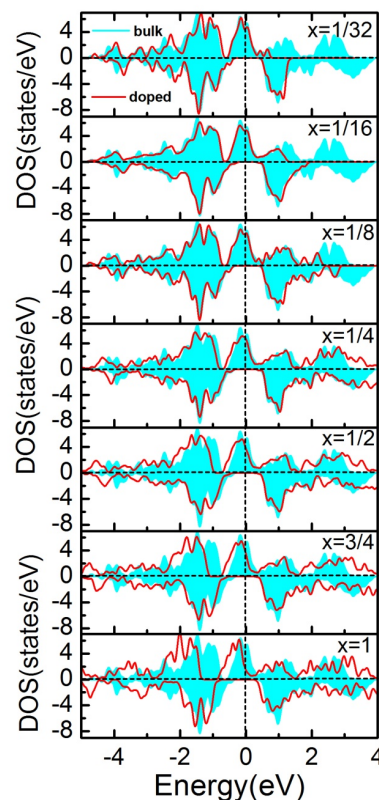


Figure 1. Total density of states (DOS) of the ordered TiZrCoIn quaternary Heusler alloy (shaded area) and the doped systems (solid line). Note that all DOS are translated to a primitive cell. Notice that x in the figure is the doping concentration.

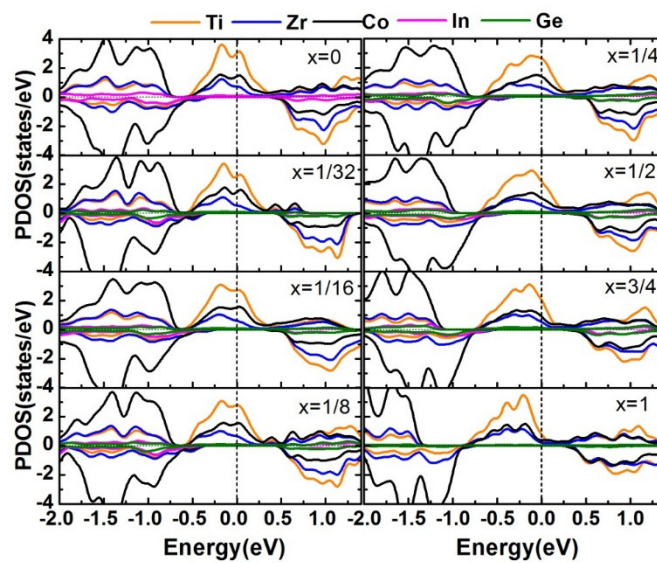


Figure 2. Partial density of states (PDOS) for the ordered TiZrCoIn quaternary Heusler alloy and the doped systems. The orange line is the atomic PDOS for Ti atom, the blue line is for the Zr atom, the black line is for the Co atom, the magenta line is for the In atom, and the olive line is for the Ge atom. Notice that x in the figure is the doping concentration.

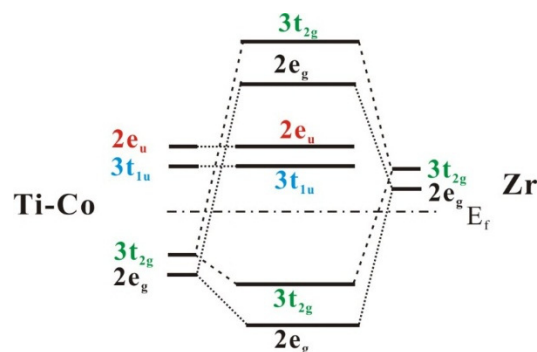


Figure 3. Schematic of the d-d hybridization of the ordered TiZrCoIn quaternary Heusler alloy.

Next, we will discuss the mixed compounds in the series $\text{TiZrCoIn}_{1-x}\text{Ge}_x$ in detail, to look for the compounds with better half-metallic stability. As shown in Figure 1, all the doped systems showed half-metallicity. The bonding states moved slightly to the low energy area. The higher the doping concentration is, the more pronounced the movement and the wider the band gaps are. The band gaps further widened from 0.914 eV to 1.13 eV at doping concentrations of 3.125%–100%. However, the Fermi levels shifted slightly from the middle of the gap to the edge of the gap. The bonding states in the spin-down channel of doped cases primarily originated from the transition metal Co with high valence, as shown in Figure 2. Meanwhile, the antibonding d states primarily came from the transition metal Ti with low valence. The d orbitals of Ti and Co atoms hybridized initially because of their identical symmetries. Then, the creating bonding d states in turn hybridized with the d orbitals of the Zr atoms. The outlines of the d states near the Fermi levels of Ti, Zr, and Co were nearly identical, especially those of Ti and Co. Therefore, Ti, Co, and Zr had intense interactions. After the addition of the doped element Ge, the number of sp valence electrons of the parent compound increased, and the increase indirectly enhanced d-d hybridization. The d-d hybridization dominated the half-metallicity of the compounds. Nonetheless, increase in total spin moment and energy band gap depend on the sp atoms. This dependence plays a substantial role in the RKKY exchange interaction.

4. Conclusions

The effects of doping on the electronic and magnetic properties of the quaternary Heusler alloy TiZrCoIn with half-metallicity were investigated with first-principles calculations based on DFT. The results showed that all the doped compounds carry negative formation energies and thus can be formed during the growth of the TiZrCoIn compound. The formation energy decreased with doping concentration. It was found that the formation energy was at its lowest value (-1.13 eV) when $x=1$. Namely, the quaternary Heusler alloy TiZrCoGe derived from doping showed stable half-metallicity. In all the cases, a wide spin-minority band gap was observed at the Fermi level, and the gap widened as the doping concentration increased. The Fermi level was located in the middle of the broadened gap, and a peak at the Fermi level was detected in the spin majority channel when x was 0.75. Thus, the compound TiZrCoIn_{0.25}Ge_{0.75} showed high half-metallic stability. The total magnetic moments of the doped compounds followed the $M_t = Z_t - 18$ SP rule, increasing from $2 \mu_B$ to $3 \mu_B$ linearly with doping concentration. The d-d hybridization among Ti, Zr, and Co dominated the half-metallicity, and sp atoms (In and Ge) played an important role in the RKKY exchange interaction.

Author Contributions: Methodology, Y.C.; software, W.Y. and B.W. (Bo Wu); formal analysis, B.W. (Bin Wang) and S.C.; investigation, Y.C. and D.L.; data curation, H.H. and X.Q.; writing—original draft preparation, S.C. and B.W. (Bin Wang); writing—review and editing, Y.C. and B.W. (Bo Wu)

Funding: This research was funded by the key projects of the tripartite foundation of the Guizhou Science and Technology Department (Grant No. [2017]7041), the Natural science research project of Guizhou provincial department of education (Grant No. [2017]288), the Key Projects of the Tripartite Foundation of Guizhou Science and Technology Department (Grant No. [2015]7696), and the project of the creative research groups of Guizhou Province of China (Grant No. [2016]048).

Acknowledgments: We are really grateful to the cloud computing platform at Guizhou University and the CNROCK HOLE BLACKHOLE high density computing platform for computing support.

Conflicts of Interest: The authors declare no conflict of interest.

References

- Ohnuma, Y.; Matsuo, M.; Maekawa, S. Spin transport in half-metallic ferromagnets. *Phys. Rev. B.* **2016**, *94*, 184405. [[CrossRef](#)]
- Griffin, S.M.; Neaton, J.B. Prediction of a new class of half-metallic ferromagnets from first principles. *Phys. Rev. Mater.* **2017**, *1*. [[CrossRef](#)]
- Kourov, N.I.; Marchenkov, V.V.; Belozerova, K.A.; Weber, H.W. Specific features of the electrical resistivity of half-metallic ferromagnets Fe₂MeAl (Me = Ti, V, Cr, Mn, Fe, Ni). *J. Exper. Theor. Phys.* **2014**, *118*, 426. [[CrossRef](#)]
- Sun, M.; Ren, Q.; Zhao, Y.; Wang, S.; Yu, J. Magnetism in transition metal-substituted germanane: A search for room temperature spintronic devices. *J. Appl. Phys.* **2016**, *119*, 666. [[CrossRef](#)]
- Li, S.; Takahashi, Y.K.; Sakuraba, Y.; Chen, J.; Furubayashi, T.; Mryasov, O.; Faleev, S.; Hono, K. Current-perpendicular-to-plane giant magnetoresistive properties in Co₂Mn(Ge_{0.75}Ga_{0.25})/Cu₂TiAl/Co₂Mn(Ge_{0.75}Ga_{0.25}) all-Heusler alloy pseudo spin valve. *J. Appl. Phys.* **2016**, *119*, 093911. [[CrossRef](#)]
- Galanakis, I.; Özdoğan, K.; Şaşıoğlu, E. Spin-filter and spin-gapless semiconductors: The case of Heusler compounds. *AIP Adv.* **2016**, *6*, 055606. [[CrossRef](#)]
- Wang, Y.; Ramaswamy, R.; Yang, H. FMR-related phenomena in spintronic devices. *J. Phys. D. Appl. Phys.* **2018**, *51*, 27. [[CrossRef](#)]
- Feng, Y.; Cui, Z.; Wei, M.S.; Wu, B. Spin-polarized quantum transport in Fe₄N based current-perpendicular-to-plane spin valve. *App. Surf. Sci.* **2019**, *499*, 78–83. [[CrossRef](#)]
- Wang, X.T.; Cheng, Z.X.; Wang, W.H. L₂₁ and XA Ordering Competition in Hafnium-Based Full-Heusler Alloys Hf₂VZ (Z = Al, Ga, In, Tl, Si, Ge, Sn, Pb). *Materials* **2017**, *10*, 1200. [[CrossRef](#)]
- Gregor, F.; Perter, K. Ternary semiconductors NiZrSn and CoZrBi with half-Heusler structure: A first-principles study. *Phys. Rev. B.* **2016**, *94*, 075203.

11. Barman, C.K.; Alam, A. Topological phase transition in the ternary half-Heusler alloy ZrIrBi. *Phys. Rev. B.* **2018**, *97*, 075302. [[CrossRef](#)]
12. Galanakis, I. Theory of Heusler and Full-Heusler Compounds. *Springer Series in Materials Science.* **2016**, *222*, 3–36.
13. Palmstrom, C.J. Heusler compounds and spintronics. *Prog. Cryst. Growth. Chara. Mater.* **2016**, *2*, 371. [[CrossRef](#)]
14. Oliynyk, A.O.; Antono, E. High-Throughput Machine-Learning-Driven Synthesis of Full-Heusler Compounds. *Chem. Mater.* **2016**, *28*, 20. [[CrossRef](#)]
15. Anjami, A.; Boochani, A.; Elahi, S.M.; Akbari, H. Ab-initio study of mechanical, Half-metallic and optical properties of Mn_2ZrX ($X = Ge, Si$) compounds. *Results Phys.* **2017**, *7*, 3522–3529. [[CrossRef](#)]
16. Ashis, K.; Srikrishna, G.; Rudra, B.; Subbhradip, G.; Biplab, S. New quaternary half-metallic ferromagnets with large Curie temperatures. *Sci. Reports* **2017**, *7*, 1803.
17. Jafari, K.; Ahmadian, F. First-principles Study of Magnetism and Half-Metallic Properties for the Quaternary Heusler Alloys $CoRhYZ$ ($Y = Sc, Ti, Cr, \text{ and } Mn; Z = Al, Si, \text{ and } P$). *J. Super. Novel. Magn.* **2017**, *14*, 1–10. [[CrossRef](#)]
18. Bahramian, S.; Ahmadian, F. Half-metallicity and magnetism of quaternary Heusler compounds $CoRuTiZ$ ($Z = Si, Ge, \text{ and } Sn$). *J. Magn. Magn. Mater.* **2017**, *424*, 122–129. [[CrossRef](#)]
19. Rani, D.; Suresh, E.K.G.; Yadav, A.K.; Jha, S.N.; Varma, D.M.R.; Alam, A. Structural, electronic, magnetic, and transport properties of the equiatomic quaternary Heusler alloy $CoRhMnGe$: Theory and experiment. *Phys. Rev. B.* **2017**, *96*, 184404. [[CrossRef](#)]
20. Wang, X.T.; Cheng, Z.X.; Liu, G.D. Rare earth-based quaternary Heusler compounds $MCoVZ$ ($M = Lu, Y; Z = Si, Ge$) with tunable band characteristics for potential spintronic applications. *IUCrJ* **2017**, *4*, 758–768. [[CrossRef](#)]
21. Li, Y.P.; Liu, G.D.; Wang, X.T.; Liu, E.K. First-principles study on electronic structure, magnetism and half-metallicity of the $NbCoCrAl$ and $NbRhCrAl$ compounds. *Results Phys.* **2017**, *7*, 2248–2254. [[CrossRef](#)]
22. Kallmayer, M.; Elmers, H.J.; Balke, B.; Wurmehl, S.; Emmerling, F. Magnetic properties of $Co_2Mn_{1-x}Fe_xSi$ Heusler alloys. *J. Phys. D: Appl. Phys.* **2006**, *39*, 786. [[CrossRef](#)]
23. Alijani, V.; Ouardi, S.; Fecher, G.H.; Jürgen, W.; Naghavi, S.S.; Kozina, X.; Stryganyuk, G.; Felser, C.; Ikenaga, E.; Yamashita, Y.; et al. Electronic, structural, and magnetic properties of the half-metallic ferromagnetic quaternary Heusler compounds $CoFeMnZ$ ($Z = Al, Ga, Si, Ge$). *Phys. Rev. B.* **2011**, *73*, 2022–2399.
24. Özdoğan, K.; Şaşıoğlu, E.; Galanakis, I. Slater–Pauling behavior in $LiMgPdSn$ -type multifunctional quaternary Heusler materials: Half-metallicity, spin-gapless and magnetic semiconductors. *J. Appl. Phys.* **2013**, *113*, 323-R. [[CrossRef](#)]
25. Feng, Y.; Chen, H.; Yuan, H.; Zhou, Y.; Chen, X. The effect of disorder on electronic and magnetic properties of quaternary Heusler alloy $CoFeMnSi$ with $LiMgPbSb$ -type structure. *J. Magn. Magn. Mater.* **2015**, *378*, 7–15. [[CrossRef](#)]
26. Yang, G.; Li, D.; Wang, S.; Ma, Q.; Liang, S.; Wei, H.; Han, X.; Hesjedal, T.; Ward, R.; Kohn, A. Effect of interfacial structures on spin dependent tunneling in epitaxial $L10\text{-FePt}/MgO/FePt$ perpendicular magnetic tunnel junctions. *J. Appl. Phys.* **2015**, *117*, 083904. [[CrossRef](#)]
27. Feng, Y.; Xu, X.; Cao, W.; Zhou, T. Investigation of cobalt and silicon co-doping in quaternary Heusler alloy $NiFeMnSn$. *Comp. Mater. Sci.* **2018**, *147*, 251–257. [[CrossRef](#)]
28. Han, J.; Gao, G. Large tunnel magnetoresistance and temperature-driven spin filtering effect based on the compensated ferrimagnetic spin gapless semiconductor Ti_2MnAl . *Journal Title* **2018**, *113*, 102402. [[CrossRef](#)]
29. Aron-Dine, S.; Pomrehn, G.S.; Pribram-Jones, A.; Laws, K.J.; Bassman, L. First-principles investigation of structural and magnetic disorder in $CuNiMnAl$ and $CuNiMnSn$ Heusler alloys. *Phys. Rev. B.* **2017**, *95*, 024108. [[CrossRef](#)]
30. Hu, Y.; Zhang, J.M. First-principles study on the thermodynamic stability, magnetism, and half-metallicity of full-Heusler alloy Ti_2FeGe (001) surface. *Phys. Lett. A.* **2017**, *381*, 1592–1597. [[CrossRef](#)]
31. Feng, Y.; Wu, B.; Yuan, H.; Chen, H. Structural, electronic and magnetic properties of $Co_2MnSi/Ag(100)$ interface. *J. Alloy. Compd.* **2015**, *623*, 29–35. [[CrossRef](#)]
32. Feng, Y.; Chen, X.; Zhou, T.; Yuan, H.; Chen, H. Structural stability, half-metallicity and magnetism of the $CoFeMnSi/GaAs(001)$ interface. *Appl. Surf. Sci.* **2015**, *346*, 1–10. [[CrossRef](#)]

33. Zhang, S.; Jin, Z.; Liu, X.; Zhao, W.; Lin, X.; Jing, C.; Ma, G. Photoinduced terahertz radiation and negative conductivity dynamics in Heusler alloy Co_2MnSn film. *Opt. Lett.* **2017**, *42*, 3080. [[CrossRef](#)]
34. Chen, Y.; Wu, B.; Yuan, H.K.; Feng, Y.; Chen, H. The defect-induced changes of the electronic and magnetic properties in the inverse Heusler alloy Ti_2CoAl . *J. Solid. State. Chem.* **2015**, *221*, 311. [[CrossRef](#)]
35. Branford, W.R.; Singh, L.J.; Barber, Z.H.; Kohn, A.; Petfordlong, A.K. Temperature insensitivity of the spin-polarization in Co_2MnSi films on GaAs (001). *New. J. Phys.* **2016**, *9*, 224. [[CrossRef](#)]
36. Pradines, B.; Arras, R.; Abdallah, I.; Biziere, N.; Calmels, L. First-principles calculation of the effects of partial alloy disorder on the static and dynamic magnetic properties of Co_2MnSi . *Phys. Rev. B.* **2017**, *95*, 094425. [[CrossRef](#)]
37. Hu, B.; Moges, K.; Honda, Y.; Liu, H.X.; Uemura, T.; Yamamoto, M.; Inoue, J.I.; Shirai, M. Temperature dependence of spin-dependent tunneling conductance of magnetic tunnel junctions with half-metallic Co_2MnSi electrodes. *Phys. Rev. B.* **2016**, *94*, 094428. [[CrossRef](#)]
38. Andrieu, S.; Neggache, A.; Hauet, T.; Devolder, T.; Hallal, A.; Chshiev, M.; Bataille, A.M.; Fèvre, P.; Bertran, F. Direct evidence for minority spin gap in the Co_2MnSi Heusler compound. *Phys. Rev. B.* **2016**, *93*, 094417. [[CrossRef](#)]
39. Yan, P.L.; Zhang, J.M.; Xu, K.W. The structural, electronic and magnetic properties of quaternary Heusler alloy TiZrCoIn . *Soli. State. Commu.* **2016**, *231–232*, 64–67. [[CrossRef](#)]
40. Perdew, J.P.; Burke, K.; Ernzerhof, M. Generalized gradient approximation made simple. *Phys. Rev. Lett.* **1996**, *77*, 3865. [[CrossRef](#)]
41. Noemí, H.H.; Joaquín, O.C.; Martynov, Y.B.; Nazmitdinov, R.G.; Frontera, A. DFT prediction of band gap in organic-inorganic metal halide perovskites: An exchange-correlation functional benchmark study. *Chem. Phys.* **2019**, *516*, 225–231.
42. Garcia, A.; Junquera, J.; Portal, D.S.; Soler, J.M. Electronic Structure Calculations with Localized Orbitals: The Siesta Method. *Spri. Neth.* **2005**, 77–91.



© 2019 by the authors. Licensee MDPI, Basel, Switzerland. This article is an open access article distributed under the terms and conditions of the Creative Commons Attribution (CC BY) license (<http://creativecommons.org/licenses/by/4.0/>).